Interplay of disorder and electron-phonon coupling in models of polyacetylene

S. R. Phillpot*
Xerox Webster Research Center, Webster, New York 14580
and Center for Nonlinear Studies and Theoretical Division, Los Alamos National Laboratory, The University of California, Los Alamos, New Mexico 87545

D. Baeriswyl,†, A. R. Bishop, and P. S. Lomdahl
Center for Nonlinear Studies and Theoretical Division, Los Alamos National Laboratory, The University of California, Los Alamos, New Mexico 87545
(Received 15 September 1986)

We present, within the Su-Schrieffer-Heeger model, analytical and numerical calculations of the effects of two types of model impurities, namely bond and site, on the statics and dynamics of the lattice structure, and adiabatically associated one-electron spectrum, of *trans*-polyacetylene. For both types of impurities two or more localized electronic levels are produced, which may be in the intragap region or beyond the π-band edges (ultraband). Linear-response calculations of the induced lattice defects are in good agreement with the numerical calculations. A numerical study of kink-impurity dynamics shows that a kink may be reflected, transmitted, or trapped by the impurity depending on both the impurity strength and the topology of the impurity-induced lattice defect. A kink trapped by a site impurity of sufficient strength is found to have *no* midgap level but is supported by a level beyond the edge of the π band. We also find that the trapping of a kink by a site impurity may result in the production of a potentially long-lived polaron. Such strong electron-phonon renormalization effects on the electronic structure in the presence of disorder are also found for bond impurities, where ultraband levels may form at the expense of more localized intragap levels. Photoexcitation experiments in the defected system produce the full range of nonlinear excitations: kinks, breathers, polarons, excitons, and trapped kinks. We calculate the optical absorption spectra in typical experiments and identify extrinsic intragap absorption.

I. INTRODUCTION

It has become widely advocated[1,2] that intrinsic nonlinear excitations (sometimes termed "solitons") play a central role in understanding the structural, thermodynamic, and transport properties of polyacetylene and related polymers. This view has been supported by experimental studies and by analytic calculations on model Hamiltonians—especially the Su-Schrieffer-Heeger (SSH) Hamiltonian[3]

$$H_{\rm SSH}=\tfrac{1}{2}M\sum_n \dot{u}_n^2+\tfrac{1}{2}K\sum_n (u_n-u_{n+1})^2 - \sum_n [t_0+\alpha(u_n-u_{n+1})](c_n^\dagger c_{n+1}+c_{n+1}^\dagger c_n)\ , \tag{1}$$

and its continuum limits.[4] In Eq. (1) the first term is the lattice kinetic energy; the second term is the lattice strain energy (this arises, in an approximate way, from the effect of σ-orbital electrons); the third term is the π-orbital electronic energy. M is the mass of a (CH) unit, K is the lattice force constant, t_0 is the intrinsic transfer matrix element, and α is the electron-phonon coupling constant. u_n is the displacement of the nth carbon atom from its lattice site and $c_n^\dagger(c_n)$ creates (annihilates) a π electron at site n. Throughout this study we use the "rescaled parameters:" $t_0=2.5$ eV, $K=17.3$ eV Å^{-2} and $\alpha=4.8$ eV Å^{-1}. These correspond to a dimerization amplitude $u_0=0.1$ Å, band gap $2\Delta_0=8\alpha u_0=3.84$ eV, an electron-phonon coupling constant $\lambda=2\alpha^2/\pi t_0 K=0.34$, and a soliton coherence length $\xi=2t_0/\Delta_0=2.6$. (Throughout this paper we assume positive Δ_0 and u_0 without loss of generality—these quantities are related by $\Delta_0=4\alpha u_0$.) The parameter values are chosen largely for computational convenience, but also for comparison with earlier numerical studies.[5]

Evidence for the importance of nonlinear excitations comes from a number of numerical studies of the classical, zero temperature, adiabatic *dynamics*.[5–7] In particular, it has been shown[5,6] that a photoexcited electron-hole pair rapidly decays to form a kink-antikink ($K\bar{K}$) pair which, in the absence of confining mechanisms, breaks up to separating K and $\bar{K}$ in $\lesssim 0.1$ psec. (For these parameters the $2k_F$ optical phonon period is numerically found to be $\simeq 0.04$ psec; our numerical time step is 0.001 psec.) We have shown in previous studies[6,8] that a neutral nonlinear excitation—a "breather"—is also produced in such an event, and we have argued that this is one mechanism for producing near-band-edge photoinduced photoabsorption as observed in *trans*-polyacetylene.[9]

Although it is well known that "pristine" samples of polyacetylene contain a non-negligible density of defects (from, e.g., cross-linking, complex morphological effects, or extrinsic impurities), most previous work has considered only defect-free systems. Experimentally the electrical conductivity can be varied on doping, undoping, and compensation, systematically and reversibly over approximately 13 orders of magnitude. This indicates that the

dopant impurities are typically nonsubstitutional and chemically nonreactive with the σ bands of the polymer backbone. (There are exceptions, e.g., Br or F substitution.[10]) We will not consider here any *direct* effects on the ionic mass or elastic terms in Eq. (1). Clearly any quasirealistic model must include the effects of impurities for a full understanding of the transport phenomena of the real system. Furthermore, for the soliton model to be relevant in real materials it is not sufficient to merely show that nonlinear excitations are robust in the defected system, but it is also essential that physically reasonable production mechanisms be identified.

In this paper the adiabatic nonlinear dynamics are studied in the presence of two model impurities. The "site impurity" is modeled by a term, added to the SSH Hamiltonian, which couples to a single lattice site.[11] This can be viewed as simulating the bonding of an orbital of a dopant impurity to the π bond of a single carbon atom, to complex morphological effects such as the presence of cross linking between chains and hybridization, or to the *short*-range Coulomb potential of a charged impurity.[12] The "bond impurity" is represented[13] by a local variation of the transfer matrix element in Eq. (1). This may model intrinsic defects of the system, such as *cis*-like segments within a *trans*-polyacetylene chain, the presence of amorphous regions within the crystalline structure, or chain bends and breaks.

The ground state of the Hamiltonian (1) with one electron per site (i.e., in the half-filled band) is dimerized, $u_n=(-1)^n u_0$, and exhibits a gap $2\Delta_0=8\alpha u_0$ separating the extended states of the filled valence band from those of the empty conduction band.[3] As discussed in Secs. II A and II B, adding an impurity of either type can produce localized electronic states in the gap ("intragap states"), as well as below the valence band and above the conduction band ("ultraband states"). A site impurity always produces both a single intragap and a single ultraband state. For a bond impurity the localized states always occur in pairs, symmetrically located with respect to midgap. A pair of ultraband states is produced if the impurity strengthens a bond, whereas a pair of intragap states occurs if the impurity either strengthens a weak bond or weakens a strong bond.

Due to the electron-phonon coupling the impurity-induced change in electronic structure is accompanied by a distortion of the lattice around the impurity. This lattice relaxation in turn tends to localize still further the electronic impurity states. For sufficiently strong impurities, we also observe "catastrophic" renormalization in which localized intragap levels become unstable in favor of ultraband levels.

A complicated interplay between intrinsic nonlinearity and extrinsic impurity potential takes place in the presence of nonlinear excitations.[14] The kink, being a topological excitation, must be stable in the presence of impurities but nevertheless can be strongly deformed locally. Indeed, for a sufficiently strong site impurity ($|V_0| \gtrsim \Delta_0$), we find a new type of kink—a "trapped kink"—which has *no* midgap electronic state; rather, it is accompanied by an ultraband state which derives its parentage from the impurity. In kink-impurity interactions a kink can be transmitted or reflected and, in the case of the site impurity, trapped.

The polaron[15] and breather are not topologically elementary excitations, but we find that they are copiously produced in photoexcitation of defected systems. We also find that an "exciton," unstable in the SSH model, can be produced. Furthermore, due to the presence of intragap states the threshold for photogeneration of kink-antikink pairs is reduced as compared to the threshold energy $2\Delta_0$ of the undefected system, thus providing an additional mechanism to the traditional Urbach fluctuation-induced intragap absorption.[16]

In Sec. II we use a simple continued fraction scheme to find the location of the localized energy levels induced by the defects. In Sec. III we use a Green's-function resolvent technique to calculate the linear approximation to the induced lattice relaxation. In Sec. IV the above results are confirmed numerically for the case of a site impurity. In Sec. V we show that a site impurity may reflect, transmit, or trap a propagating kink. Section VI deals with polarons and bipolarons in the site-defected system and it is shown that the bipolaron decays to a free kink and a trapped antikink. In Sec. VII we perform representative photoexcitation experiments in the presence of site impurities; we also calculate numerically the optical-absorption spectra. Section VIII looks at the lattice relaxation in the presence of a single bond impurity. Sections IX and X treat kink-bond impurity and polaron-bond impurity interactions and Sec. XI examines photoexcitation in the presence of a bond impurity. Section XII contains a discussion and our conclusions including their possible experimental relevance. The Appendixes A and B contain more details of the analytical calculations and Appendix C of our numerical procedure. Some preliminary results have already been published.[17]

II. IMPURITY STATES

We consider two types of impurities, a site impurity represented by a local potential at site m:

$$H_1=V_0 c_m^\dagger c_m \ , \tag{2}$$

and a bond impurity acting on the bond between sites m and $m+1$:

$$H_2=-W_0(c_m^\dagger c_{m+1}+c_{m+1}^\dagger c_m) \ . \tag{3}$$

The SSH Hamiltonian, Eq. (1), has electron-hole symmetry. Indeed, the electronic part of $H_{\rm SSH}$ changes sign under the canonical transformation $c_n\rightarrow(-1)^n c_n$ which implies that all electronic levels with nonzero energy occur in pairs at $\pm\varepsilon_\nu$. A bond impurity does not affect this symmetry and any bound states induced by H_2 likewise occur in pairs. On the other hand, a site impurity represented by H_1 destroys the electron-hole symmetry. Therefore the two types of impurities are expected to have markedly different effects both on the electronic states and on the lattice. In this section we restrict ourselves to discussing the modifications of the electronic structure: We assume the lattice to be perfectly dimerized and neglect any lattice relaxation.

A. Site impurity

The case of a single site impurity has been studied in Ref. 11 by summing the expansion of the resolvent operator $G(z)\equiv(z-H)^{-1}$ in powers of the impurity potential to all orders. The impurity levels can also be derived by using a continued-fraction approach, as shown in Appendix A. For a homogeneously dimerized structure with alternating bonds A and B, we find impurity states at

$$E_{\pm}=\pm\mathrm{sgn}(V_0)\,|\,(t_A^2+\tfrac{1}{4}V_0^2)^{1/2}\pm(t_B^2+\tfrac{1}{4}V_0^2)^{1/2}\,|\ , \quad (4)$$

where t_A and t_B are the two transfer matrix elements $t_0\pm\frac{1}{2}\Delta_0$. These solutions are depicted in Fig. 1 as functions of V_0. For a donor impurity ($V_0<0$) a state drops from the bottom of the conduction band into the gap while a state also detaches from the bottom of the valence band. As $|V_0|$ increases the energy of the intragap state tends asymptotically towards midgap ($E=0$), while the energy of the ultraband state decreases without bound. For an acceptor impurity ($V_0>0$) a state moves from the top of the valence band into the gap while another state emerges from the top of the conduction band. In this paper we consider donors: all results remain the same for acceptors with electrons and holes interchanged.

It is straightforward to extend this analysis to the case of two impurities at different sites.[11] For large separation two nearly degenerate levels appear in the gap. As the two sites approach each other, one level becomes deeper and the other shallower. For very small separations the deep level asymptotically approaches a value which corresponds to the impurity state of a single potential with strength $2V_0$, whereas the shallow level merges with the conduction band. This is in agreement with numerical results for an isotropically screened Coulomb potential[14] which produces several levels in the gap, all but one being very shallow. For an anisotropically screened Coulomb potential (which amounts to a reduced screening at long distance) several impurity states spread throughout the gap.[14]

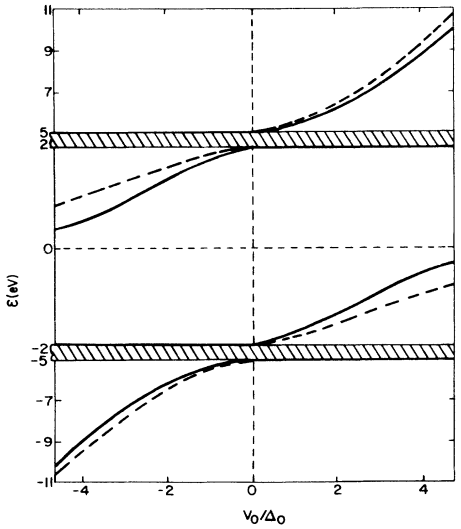

FIG. 1 Location of site impurity-induced localized electronic levels as a function of impurity strength, V_0. Dashed line is the analytic calculation of Sec. II. Solid line is the consistent numerical calculation of Sec. IV. For $V_0<0$ (a donor impurity) there is a single "intragap state" above midgap and a single "ultraband state" below the edge of the valence band.

B. Bond impurity

We assume the impurity to attack an A bond, thus replacing a single transfer element t_A by $t_E=t_A+W_0$. As shown in Appendix A there are pairs of intragap states at

$$E=\pm\{t_E^2+t_A^2-[(t_E^2-t_A^2)^2+4t_E^2t_B^2]^{1/2}\}/(2t_E)\ , \quad (5)$$

provided that the impurity either strengthens a weak bond ($t_A<|t_E|$, $t_A<t_B$) or weakens a strong bond ($t_A>|t_E|$, $t_A>t_B$). This is plausible since in both cases the bond impurity locally decreases the dimerization—indeed the limit $t_E=t_B$ corresponds topologically to a $K\bar{K}$ pair with two localized midgap states. Similarly ultraband states at

$$E=\pm\{t_E^2+t_A^2+[(t_E^2-t_A^2)^2+4t_E^2t_B^2]^{1/2}\}/(2t_E) \quad (6)$$

appear only if the impurity strengthens the bond ($t_A<|t_E|$). Again this is reasonable since the band width is locally increased. The effects of a bond impurity on the electronic structure are illustrated in Fig. 2.

III. IMPURITY-INDUCED LATTICE RELAXATION —LINEAR RESPONSE

The changes in the electronic structure and, in particular, the appearance of localized electronic states produce local lattice distortions due to the electron-phonon coupling. In this section we study the linear response of the lattice. It is convenient to discuss this problem in terms of variables $\Delta_n=2\alpha(-1)^n(u_n-u_{n+1})$ which are proportional to changes in bond lengths. Varying the expectation value of Eq. (1) with respect to Δ_n we obtain the following relation for the ground-state configuration

$$\Delta_n=2\pi t_0\lambda(-1)^n\langle c_n^{\dagger}c_{n+1}+c_{n+1}^{\dagger}c_n\rangle\ , \quad (7)$$

where a factor of 2 has been included for the spin summation. Equation (7) is generally valid even upon adding the impurity potentials H_1,H_2 to the Hamiltonian. The right-hand side (rhs) of Eq. (7) is evaluated using the relation (valid at zero temperature)

$$\langle c_nc_{n+1}^{\dagger}\rangle=\int_{-\infty}^{\infty}\frac{dE}{2\pi}G_{n+1,n}(iE)\ , \quad (8)$$

where

$$G_{mn}(z)=\langle m\,|\,(z-H_{\mathrm{el}})^{-1}\,|\,n\rangle \quad (9)$$

is the electronic Green's function, H_{el} representing the electronic part of the Hamiltonian, and $|n\rangle$ a Wannier state at site n. Evaluating it for the pure system with homogeneous dimerization ($\Delta_n=\Delta_0$) and inserting it into Eq. (7) yields the usual gap equation.[3] The additional distortions introduced by the impurities are obtained from the equation

$$\Delta_n-\Delta_0=2t_0\lambda(-1)^n\int_{-\infty}^{\infty}dE[G_{n+1,n}(iE)-G_{n+1,n}^0(iE)]\ , \quad (10)$$

where G and G^0 are the Green's functions for the defected and pure system, respectively. [For the cases considered in the following, the Green's functions are symmetric, $G_{mn}(z)=G_{nm}(z)$.] The linear response of the lat-

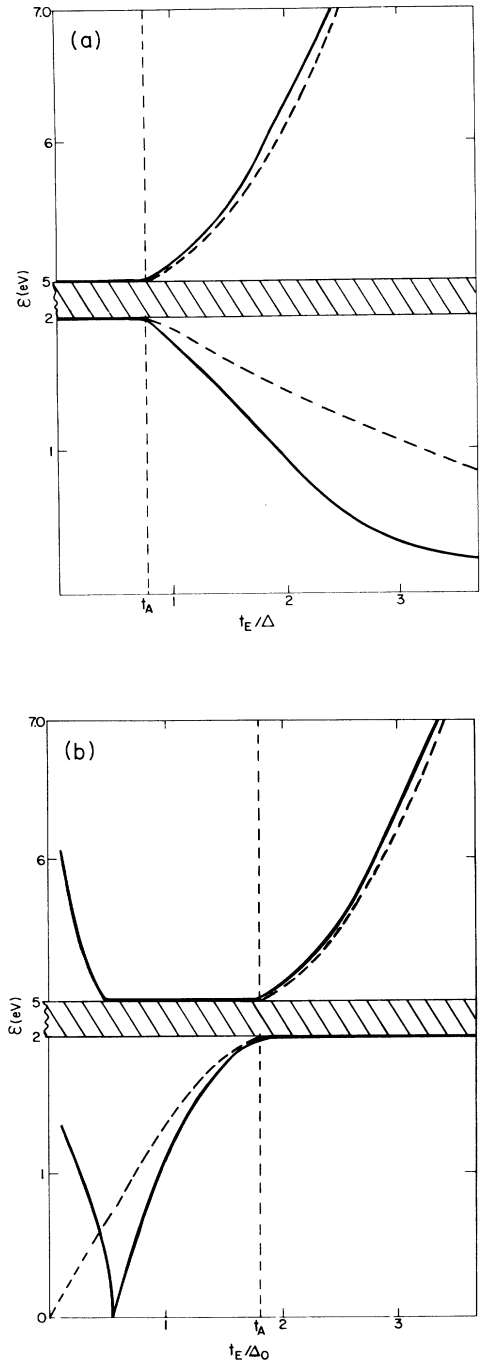

FIG. 2. Location of bond impurity-induced localized electronic levels as a function of the defected bond strength $t_E = t_A + W_0$: (a) Defect on a weak bond ($t_A < t_B$): dashed line is the analytic calculation of Sec. II; there is both a pair of intragap and a pair of ultraband levels if the weak bond is strengthened ($|t_E| > t_A$) but *no* localized levels if the bond is weakened; solid line is the consistent numerical calculation of Sec. VIII. (b) Defect on a strong bond ($t_A > t_B$): dashed line is the analytic calculation of Sec. II; if the bond is weakened ($|t_E| < t_A$) there is a pair of intragap states; if the bond is strengthened ($|t_E| > t_A$) there is a pair of ultraband states; solid line is the consistent numerical solution of Sec. VIII.

tice is obtained by calculating both G and G^0 for homogeneous dimerization. This is carried out in Appendix B. Before stating the results, we notice that the Hamiltonian (including impurity potentials) is invariant with respect to a translation $u_n \rightarrow u_n + v$. As shown in the Appendixes both impurity types induce rigid displacements u_+ and u_- far to the right and far to the left of the impurity, respectively. Using the freedom to fix an arbitrary constant displacement we choose $u_+ + u_- = 0$. Then the results can be generally written as

$$u_n = \begin{cases} u_a + (-1)^n u_0 (1 + y_n), & n > m \\ -u_a + (-1)^n u_0 (1 + y_n), & n \leq m \end{cases}, \tag{11}$$

where u_a describes the overall (acoustic) lattice expansion (or contraction) and y_n the localized lattice distortions around the impurity which decrease as $[(\xi - 1)/(\xi + 1)]^{|n-m|}$. For small impurity potentials the lattice relaxation increases linearly with the potential strength for a bond impurity but quadratically in the case of a site impurity. Equation (11) corresponds to a chain with free ends. For the boundary conditions used in the numerical studies (periodic or fixed boundary conditions), the acoustic deformations are strongly suppressed. In order to compare the analytical results for the linear lattice relaxation with the numerical results for the full lattice relaxation we show in Figs. 3 and 4 the order parameter Δ_n rather than the displacements u_n. The lattice relaxation in the vicinity of a site impurity is illustrated in Fig. 3. The behavior is smooth except close to the impurity where a strong kink- or antikink-like step is produced depending on $\sigma_m = (-1)^m$. Figure 4 shows the "polaronlike" lattice distortion around a bond impurity. The order parameter is locally enhanced either if the impurity strengthens a strong bond ($W_0 > 0$, m even) or if it weakens a weak bond ($W_0 < 0$, m odd). In the other two cases the order parameter is locally reduced. In addition to the local structure we find an overall expansion $2u_a > 0$ if $W_0 > 0$ and an overall contraction $2u_a < 0$ if $W_0 < 0$.

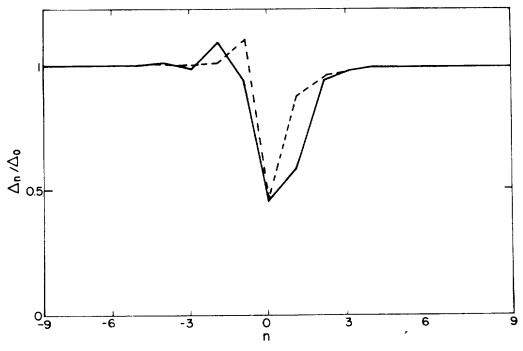

FIG. 3. Lattice relaxation around a site impurity at $m = 0$ for an impurity strength $V_0 = 2.5\Delta_0$. Dashed line is analytic results of Sec. III; solid line is the consistent numerical calculation of Sec. IV.

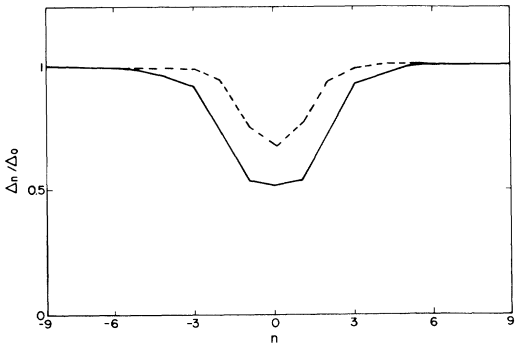

FIG. 4. Lattice relaxation around a bond impurity for $m=0$ (i.e., at a strong bond) for an impurity strength $W_0=-\Delta_0$. Dashed line is analytic results of Sec. III; solid line is the consistent numerical calculation of Sec. VIII.

IV. FULL LATTICE RELAXATION AROUND A SITE IMPURITY

There are two general classes of boundary conditions for a system of length N, which are conveniently discussed in terms of staggered displacements $\tilde{u}_n=(-1)^n u_n/u_0$. On a "ring" the first and Nth sites are coupled directly via both electronic and lattice terms in the Hamiltonian. For an even length ring, strictly periodic-boundary conditions in the dimerization amplitude may be applied, $\tilde{u}_1=\tilde{u}_N$. For an odd length ring on which there is a single kink, antiperiodic boundary conditions must be applied, $\tilde{u}_1=-\tilde{u}_N$, breaking the electron-hole symmetry to order $1/N$. For a chain, on the other hand, the $n=1$ site is coupled only to the $n=2$ site and the $n=N$ site is coupled only to the $n=N-1$ site, there being no direct coupling between the sites 1 and N.

We have used three types of chain boundary conditions in our studies: (i) "free boundary conditions:" the two end sites are coupled only to their single nearest neighbors, with no external constraints applied to them; (ii) "pressure boundary conditions:" to conserve the total length of the system the term $(4\alpha/\pi)(\tilde{u}_N-\tilde{u}_1)$ is added to the Hamiltonian; (iii) "fixed boundary conditions:" the two end sites are slaved to their neighbors, $\tilde{u}_1=\tilde{u}_2$, $\tilde{u}_N=\tilde{u}_{N-1}$. For the chains with free boundary conditions [cf. Eq. (11)], there is a strong tendency to produce acoustic phonons at the chain ends which propagate into the interior and may permit topological changes of conformation within the system. For example, an odd length chain with a single *kink* at its center and weak bonds at its ends induces a pair of antikinks at the ends. Driven by the phonon field these may propagate along the chain, leading to a $K\bar{K}$ annihilation and leaving a single *antikink* and strong bonds at the chain ends. Fixed and pressure boundary conditions do not produce acoustic phonons and do not induce such conformation changes. The long-range acoustic relaxation accompanying free boundary conditions is expected to significantly renormalize the energy of conformational (e.g., defect) distortions, as is well known in the context of semiconductors.[18]

In the studies involving a single kink we use chains with fixed boundary conditions. All other studies are performed on even length rings with periodic boundary conditions.

The analytic calculations of Sec. III do not treat the electron-phonon coupling in a fully self-consistent manner; this can, in general, only be done numerically. Here we integrate the equations of motion derived from the SSH Hamiltonian on a large ring (98 sites) and remove energy (by setting the velocity to zero at each time step; for details of this procedure see Appendix C) until the total energy reaches a minimum. We assume that this is the fully self-consistent solution to the defect-modified SSH Hamiltonian. At time $t=0$ we have the same level of consistency as in the analytic calculation and find quantitative agreement between the analytically and numerically calculated locations of the impurity states. We find that the equilibrium, relaxed lattice configuration, and electronic band structure is typically achieved within 0.1—0.2 psec. The location of the impurity states is qualitatively similar to those calculated analytically; the fully self-consistent electronic levels being deeper, i.e., more localized, than those calculated in the linear approximation (cf. Fig. 1).

In agreement with the linear-response calculation of Sec. III, we find that the localized state is accompanied by a localized lattice distortion, consisting of a sharp step on the weak bond neighboring the impurity and a tail ($\sim\xi$) at the other side of the impurity. This means that of an impurity on an even numbered site there is an antikink-like step and a kink-like tail. Assignment of the impurity-induced lattice defect as a bound state of two excitations may seem surprising, but is justified by the numerical observation that the wave function of the ultraband state is localized around the step while that for the intragap state is localized around the tail. This being so, under suitable conditions, it might be possible to separate the step from its tail, producing a topological kink-antikink pair with one of the kinks supported not by a midgap state, but by the ultraband state. Indeed, in the next section we shall find that this possibility is realized and that it has important consequences for the dynamics of the *site*-defected system.

V. INTERACTION BETWEEN A KINK AND A SITE IMPURITY

A. Statics

In this subsection we start from an impurity and a kink on nearby sites and allow the system to relax by removing kinetic energy until an energy minimum is reached. Analytical work in the continuum limit[11] and numerical calculations for a discrete chain[14] indicate that a site impurity has a weak effect on a kink but a strong effect on an antikink or vice versa. If we limit ourselves to the case of a kink this means that the interaction with a site impurity depends on whether the impurity is on an even or odd site. Our discrete lattice simulations show that these two cases are indeed qualitatively distinct and these are described separately below.

(1) *Impurity on an odd site.* The kink midgap state has vanishing wave-function amplitudes on odd numbered

sites and thus we expect that it is barely affected by the impurity potential. We indeed find that the midgap state and the intragap impurity state interfere only very weakly.

(2) *Impurity on an even site.* In this case one expects that the two intragap states interfere, since the midgap state has a nonvanishing amplitude on the impurity site. Our initial configuration of kink and impurity has an electronic spectrum in which the kink intragap level is shifted from midgap, and the impurity has an ultraband but no intragap level [(i) in Fig. 5]. On relaxing the system, for a weak impurity $|V_0| \lesssim \Delta_0$, there is simply a quantitative renormalization of these levels: the kink intragap state moves closer to midgap and the impurity ultraband level deepens. There is still, however, no intragap impurity state. The lattice distortions of the kink and impurity do appear to interact only weakly and the relaxed lattice is a linear superposition of the distortions of the kink and impurity.

Relaxation in the presence of a strong impurity, $|V_0| \gtrsim \Delta_0$, is qualitatively different. The kink becomes trapped around the impurity with a width of only one or two lattice sites. This trapped kink is supported by the impurity ultraband state. The kink intragap level is now redundant and may, if doubly occupied, drop back into the valence band [(ii) in Fig. 5]. If the kink level is only singly occupied, the kink and impurity intragap levels form a polaron in addition to the trapped kink. One might suppose, however, that the configuration with a *free* antikink at the center and a pair of kinks at the chain ends will be favored energetically. We find that this configuration, although energetically less favorable than kink trapping, is in fact metastable. We have made no estimate of the energy barrier between them and both may occur in the real system.

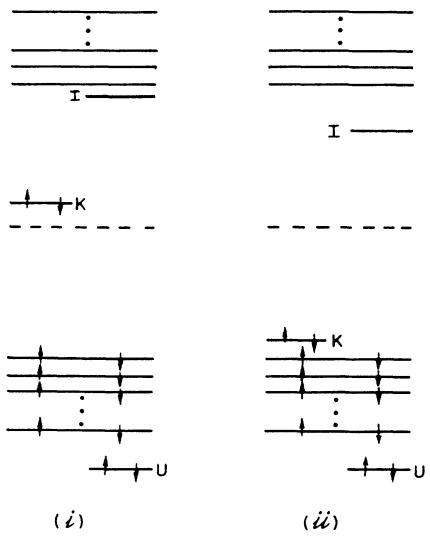

FIG. 5. Schematic of the electronic spectrum during a kink impurity interaction when the kink and impurity are in the same topological sector: (i) At $t=0$ the kink intragap level (K) is above midgap and the impurity intragap state (I) remains at the lower edge of the conduction band. There is an impurity-induced ultraband state (U) below the edge of the valence band. (ii) The ultraband impurity state (U) deepens, supporting the trapped kink and the kink ultragap state (K) drops to the valence-band edge.

B. Dynamics

The above study of the interaction of static kink and impurity is clearly not the whole story: we can expect that the dynamics of a single kink and impurity may well show new effects. To investigate these we boost a single kink towards an impurity such that before collision the kink has reached terminal velocity[6] and the impurity-induced lattice defect has substantially relaxed.

(1) *Impurity on an odd site.* For small $|V_0|$ ($\lesssim \Delta_0$) the impurity-induced lattice distortion is sufficiently small that the kink can "ride over" it. For large $|V_0|$ ($\gtrsim \Delta_0$) we have seen that for different velocities the kink can be either reflected or transmitted. Although we have not carried out systematic studies of kink-impurity dynamics, we expect that the outcome of a collision may not be a simple function of velocity. Other parameters, e.g., resonances of the kink-impurity system or the presence (or absence) of phonons may also be important to the outcome of the collision. (In ϕ^4 dynamics[19] it has been shown, for $K\bar{K}$ collisions, that there are windows of reflection within the region of transmission. Even more complex dynamics is observed for kink-breather collisions.)

(2) *Impurity on an even site.* For low $|V_0|$ ($\lesssim \Delta_0$) we again find that the impurity-induced defect can "ride over" the kink [Fig. 6(a) shows the case $V_0 \simeq 0.25\Delta_0$]. Here, however, as the kink approaches the impurity the kink "midgap" state drops below midgap. After the kink has passed through the impurity this state returns to midgap and the kink and impurity evolve independently. However, for large $|V_0|$ ($\gtrsim \Delta_0$), we find that the kink initially accelerates to a high propagation velocity (greater than the maximum uniform propagation velocity V_m in the defect-free system). However the propagation is smooth with no evidence of a kink tail structure as observed in the propagation of a single free kink.[6] On approaching the impurity (at a separation of about five lattice constants) the kink is rapidly accelerated to a very high velocity ($\gtrsim 250 V_m$) and trapped by the impurity [Fig. 6(b) shows the case of $V_0 \simeq 2.5\Delta_0$]. The kink appears to remain trapped for all times. The trapped kink is now supported by the ultraband state of the impurity and the midgap state of the free kink is redundant. For a neutral kink this midgap state is singly occupied and thus does not fall back into the valence band but, together with the intragap impurity state, forms a hole polaron. Thus in this case we have the novel situation of a donor impurity inducing a hole excitation.

The trapping of a kink results in the loss of midgap absorption, indeed the direct detection of such a trapped kink will be extremely difficult—transitions from the ultraband impurity state to the condition band have energies well above the band edge and numerically are seen to be weak. It must also be remembered that such a deep-lying ultraband state may hybridize with the σ-band electrons or form intraband resonances, the effects of which are not easy to calculate without more detailed band-structure input. These ultraband impurity levels have been theoreti-

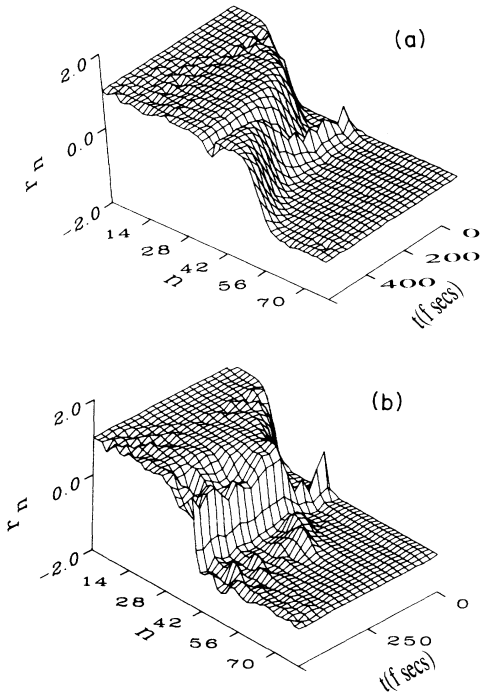

FIG. 6. Dynamics of a collision of a moving kink with a static site impurity: (a) Weak impurity, $V_0 \sim 0.25\Delta_0$, the kink rides over the impurity; (b) strong impurity, $V_0 \sim 2.5\Delta_0$, the kink is trapped by the impurity.

cally described and experimentally observed in doped semiconductors with a distinct gap below the valence band. As discussed in Ref. 20 the accompanying intragap level has the character of an antibonding "host state" (dangling bond).

VI. POLARONS AND BIPOLARONS

In the case of the undoped system, addition of an extra electron forms a polaron. In the presence of a site impurity an added electron in the intragap impurity state (a negatively charged site impurity) self-traps by increasing the localization of the impurity-induced lattice distortion. However, unlike the polaron, there may be, for sufficiently large $|V_0|$, only a single state in the gap, which derives its parentage from the intragap impurity state (see Fig. 7)—the ultraband state is also further localized.

The addition of two electrons to the pure system creates an unstable bipolaron which rapidly decays to a separated kink-antikink pair. In the presence of a site impurity, we again find that a kink-antikink pair is produced, seeded around the impurity lattice defect. Here, however, for $|V_0| \gtrsim \Delta_0$ the step evolves to a trapped antikink supported by the ultraband state while the tail evolves to a free kink, supported by the intragap impurity state which drops to midgap. This free kink is expelled at the maximum free kink velocity[6,8] by the antikink trapped at the impurity.

VII. PHOTOEXCITATION IN THE PRESENCE OF A SINGLE SITE IMPURITY

A. Adiabatic dynamics

In an earlier work we have shown that breathers (coherent nonlinear phonon packets) are produced in the photoexcitation of pristine *trans*-$(CH)_x$.[6] This results in a sub-band edge contribution to the photoinduced photoabsorption. In this section we consider photoexcitation of a single electron in the presence of a single site impurity. As representative examples we consider four simple cases of a single impurity of strength $|V_0| \sim 2.5\Delta_0$ on a 98 site ring. (We find for a weak impurity, $|V_0| \lesssim \Delta_0$, that the evolution during photoexcitation is qualitatively similar to that of the undefected system.[6] This regime will not be described further here.) In each case the initial condition is the fully-self-consistent ("relaxed", cf. Appendix C) lattice distortion and band structure. At $t=0$ the system is "photoexcited" by manually removing an electron from the highest occupied level and placing it in the appropriate unoccupied level. This level occupancy then remains fixed throughout the adiabatic dynamics. Figure 8 shows a schematic of the evolution of the energy levels and bond order for each of the four examples considered below. (Note that we have *not* attempted to incorporate selection rules for charged versus neutral soliton branches in this work.)

(1) *Empty intragap impurity state: Promotion into the intragap state.* Here we find that the impurity traps a negatively charged kink supported by the ultraband state. The intragap impurity state drops to midgap forming a free neutral antikink which is expelled by the trapped kink. The singly occupied state at the top of the valence band and the empty state at the bottom of the conduction band immediately move into the gap forming a hole polaron on the opposite side of the ring from the impurity

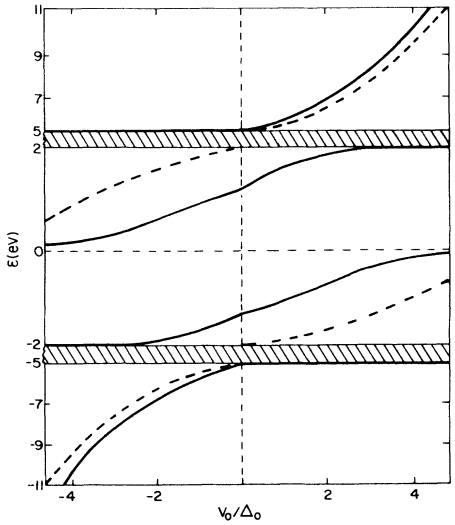

FIG. 7. Numerically calculated locations of site impurity-induced levels for a negatively charged donor impurity as a function of the impurity strength, V_0. Dashed line: "unrelaxed $t=0$ calculation; solid line: numerically consistent calculation of Sec. VI.

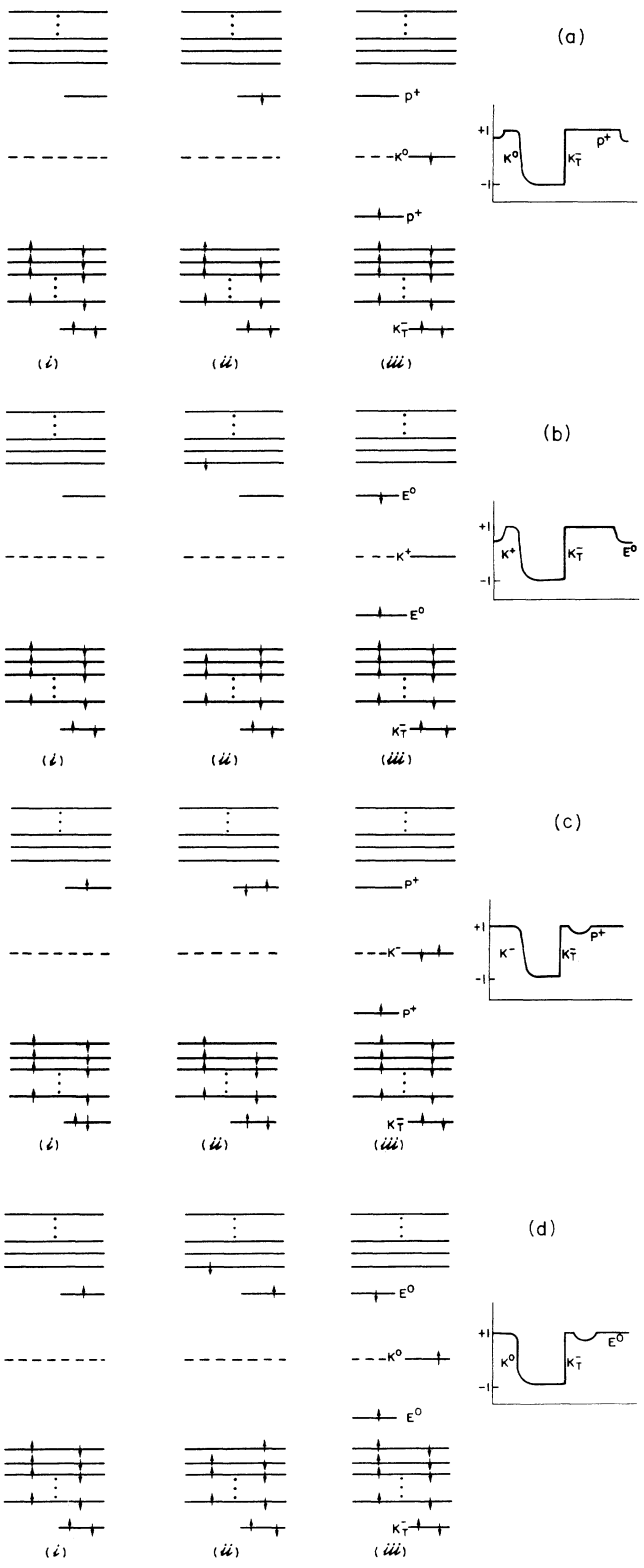

FIG. 8. Schematic of the evolution of energy levels and order parameters for four examples of photoexcitation in the presence of a site impurity. (i) Initial configuration, (ii) $t=0$ photoexcited configuration, (iii) fully evolved configuration. [(a)—(d) correspond to the four cases described in Sec. VII.]

(Fig. 9). (This apparent action at a distance should likely be attributed to adiabatic dynamics and boundary conditions employed in these calculations, and is probably not physical.)

(2) *Empty intragap impurity state: Promotion into the bottom of the conduction band.* In this case a negatively charged trapped kink and positively charged free antikink are formed in ~ 0.1 psec. The singly occupied states at the top of the valence band and the bottom of the conduction band move into the gap creating an excitonlike structure far from the impurity. The exciton is dressed by a breather, which has the electronic signature of states oscillating from the band edges deeply into the gap: the state arising from the valence band is doubly occupied, that coming from the conduction band is empty.

(3) *Singly occupied intragap impurity state: Promotion into impurity state.* Here a negatively charged free antikink is expelled by the negatively charged trapped kink. A hole polaron is formed at the impurity and is expelled from it as a "dynamic polaron"—we find no evidence for an internal oscillatory mode being excited in the polaron (Fig. 10).

(4) *Singly occupied impurity state: Promotion to the bottom of the conduction band.* A negatively charged trapped kink and a neutral free antikink form within 0.1 psec. A dynamic exciton is expelled by the impurity and a breather forms a long way from the impurity.

B. Optical absorption

With these particularly complicated dynamics it is not easy to predict what the detailed effects on the photoinduced optical absorption are. Using the techniques described elsewhere,[8] we have numerically calculated the optical absorption of the system after it has evolved for a substantial period ($\sim$ 0.3 psec) for the cases (1) and (3) in Sec. VII A. (Care must be taken in calculating the optical spectrum as $[H_1, H_{\rm SSH}]=0$ and thus H_1 contributes to neither the current operator nor to the effective electronic Hamiltonian used in the sum rule.) As preliminary input we first calculate the optical absorption of the dimerized lattice with single neutral and charged impurities ($V_0 \sim -2.5\Delta_0$). The presence of the intragap impurity level allows sub-band-edge photoabsorption arising from

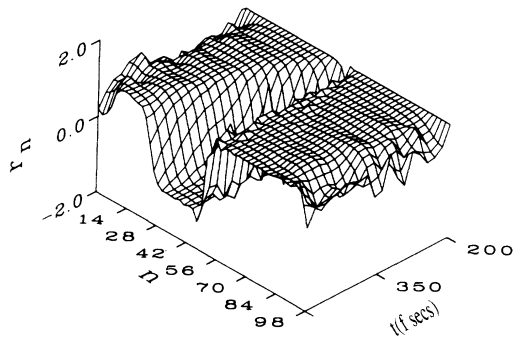

FIG. 9. Evolution of the lattice following photoexcitation of one electron from the top of the valence band into the empty intragap level of a neutral donor site impurity.

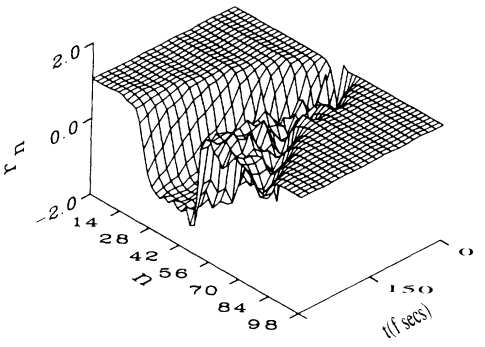

FIG. 10. Evolution of the lattice following photoexcitation of one electron from the top of the valence band into the singly occupied intragap level of a charged donor site impurity.

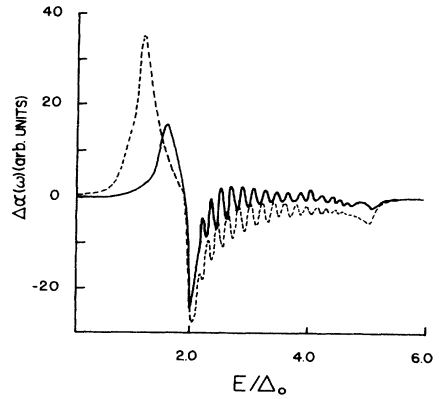

FIG. 11. Difference, $\Delta\alpha(\omega)$, between absorption of site-defected lattice ($V_0=-2.5\Delta_0$) and purely dimerized lattice. Solid line is neutral impurity; dashed line is charged impurity.

transitions into the impurity level from the valence band and, for the charged impurity, out of the impurity level into the conduction band. In Fig. 11 we show the *difference*, $\Delta\alpha(\omega)$, between the absorption of a ring with an impurity and that of the same length ring without an impurity. For the neutral impurity we see a single sub-band-edge enhancement, arising from transitions from the valence band into the impurity level. This is compensated by above-band-edge bleaching in the range $\sim(2-3)\Delta_0$. For the charged impurity the situation is similar: the sub-band-edge enhancement now comprises a strong single peak, arising from transitions into the impurity state; it also has a low-energy shoulder, arising from transitions from the singly occupied impurity intragap level into the conduction band. We see that once again there is above-band-edge bleaching, but it is more uniform in energy. This high-energy bleaching is due to the very sharp lattice distortion, the description of which requires high wave-vector, and hence high-energy, Fourier modes. In both cases the bleaching at the full bandwidth is due to the loss, on adding an impurity, of the square-root singularity in the density of states at the band edge.

In Fig. 12 we show the *difference* between the optical absorption of the photoexcited system and the dimerized system with the appropriate impurity. Below the band edge the two cases are qualitatively similar: there is a strong midgap transition involving the free kink midgap level; the peak at $\sim\Delta_0/2$ is due to transitions into the polaronic level.[21] The sub-band-edge dip (actually a bleaching for the neutral impurity) arises from the loss of absorption into the impurity state, which has now evolved to midgap. The sharp bleaching above the band edge results from the loss of the low wave-vector states needed to produce the broad polaron. For the neutral impurity there is a further bleaching over a wide energy range, arising from the large range of wave-vector states needed to describe the trapped kink. (This bleaching is largely absent in the case of the charged impurity since the step produced in the relaxation of the ground-state system is topologically similar to the trapped kink.) It is also important to note that the ultraband level only couples weakly to the continuum state of the conduction band.

C. Photoexcitation in the presence of more than one site impurity

In each of the above experiments the intragap impurity state evolves to a midgap state. However, in a more general photoexcitation experiment this need not happen. In particular for a system with a high impurity density, but optically pumped at low power, insufficient electrons are photoexcited to allow all the impurity states to form kinks, with their associated midgap states: thus the "impurity band" is largely unaffected. As a model of such an experiment we consider single electron photoexcitation in a system with 3 or 5 impurities of strength $V_0\sim2.5\Delta_0$ placed randomly on a 98 length ring.

On relaxing to a self-consistent ground state we find that if the impurities are widely spread ($\gtrsim\xi$) the electronic levels evolve independently and are almost degenerate. For closely spaced impurities ($\lesssim\xi$) the impurity wave functions overlap, lifting the electronic degeneracy and creating an "impurity band."

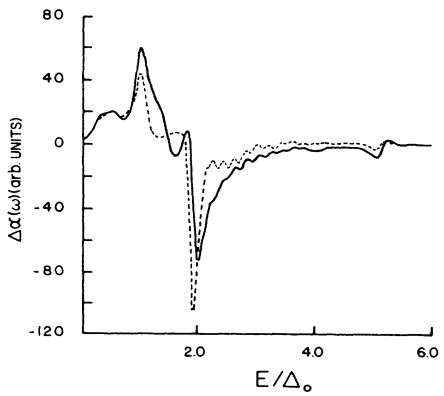

FIG. 12. Change in absorption, $\Delta\alpha(\omega)$, of the defected system following photoexcitation of an electron into the intragap level for neutral impurity, solid line, and charge impurity, dashed line.

(1) *Empty intragap states: Promotion into the bottom of the conduction band.* We find that the singly occupied states at the top of the valence band and the bottom of the conduction band are prevented from forming a $K\bar{K}$ pair (with their associated midgap states) by the presence of the intragap impurity states. Instead the system evolves to a broadened impurity band and an exciton, accompanied by a high-energy breather. It is interesting to note that all of the important dynamics occurs between two widely spaced impurities, the rest of the system acting as a "spectator." Here again the effective chain length for dynamics is essentially limited not by the physical size of the system, but rather by the impurity spacing.

(2) *Empty intragap states: Promotion into the lowest intragap state.* Here the singly occupied intragap impurity state drops below midgap and, with a second impurity state, forms (between two widely spaced impurities) a polaronic excitation. This qualitative change from impurity to polaronic electronic states is allowed by the collapse of the antikink and kink tails of a pair of closely spaced impurities, which form a pair of trapped kinks. As in case (1) of this subsection, there are a large number of intragap states—two associated with the polaronic excitation, three associated with inert impurities, and up to six other states associated with breathers.

VIII. FULL LATTICE RELAXATION AROUND A BOND IMPURITY

As in the case of the site impurity, the analytic calculations of Secs. II and III do not treat the electron-phonon coupling consistently. Numerical minimization of the energy of the bond-defected system may result in a qualitative alteration of the *electronic* spectrum of the system. As Fig. 2(b) shows, the electron-phonon coupling may result in a *delocalization* of the intragap states. This is partially compensated by an increase in the *localization* of the ultraband states. (A similar "catastrophic" Franck-Condon renormalization has been previously discussed by Anderson in the context of disordered semiconductors.[22]) Since the bond impurity induces localized levels symmetrically about midgap and since for many values of the impurity strength there are *no* intragap levels, one expects the dynamics of the system to be similar to those of the undefected model. Since the impurity is on a single bond, the induced lattice defect is symmetric and about the band center and topologically trivial (Fig. 4).

IX. KINK–BOND-IMPURITY INTERACTIONS

The outcome of kink–bond-impurity interactions is severely restricted by the electron-hole symmetry of the band structure. This keeps the kink intragap level at midgap and ensures that kink-impurity interactions mainly occur via the lattice degrees of freedom. Nevertheless, this still enables the impurity to affect the kink dynamics. Figures 13(a) and 13(b) show the dynamics of a kink launched with the same velocity at a strong bond impurity of strengths $W_0 \sim -\Delta_0/2$ and $W_0 \sim -\Delta_0$, respectively. The smaller impurity defect allows the kink to ride over it, while the stronger impurity reflects the kink.

A case of particular interest is that of $t_E = 0$, i.e., the bond defect is such that there is no electronic coupling between the m and $(m+1)$ sites (there is still of course coupling through the phonon field). This could approximate the effects of a short break in the chain or the presence of a local amorphous region. Here we find that for a wide range of kink kinetic energies and for an impurity on either a weak bond or a strong bond the kink is reflected by the defect. This suggests that in the real material kinks may be confined over short segments of the system.

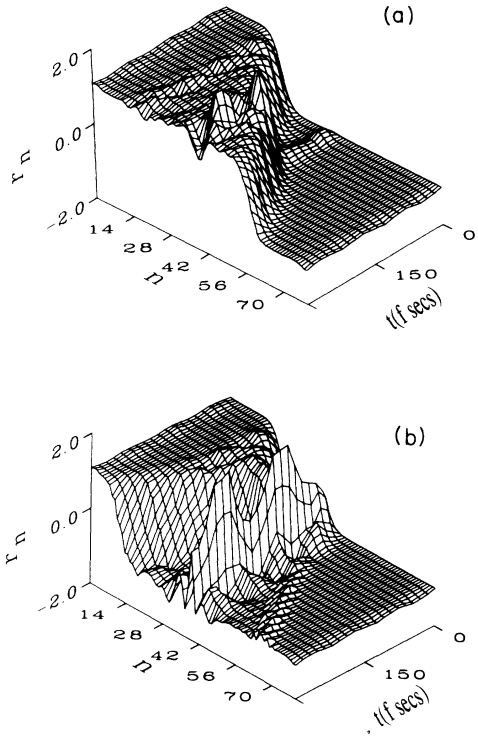

FIG. 13. Dynamics of a moving kink with a strong bond impurity of strength: (a) $W_0 \sim -\Delta_0/2$ and (b) $W_0 \sim -\Delta_0$.

X. POLARON-BOND IMPURITY INTERACTIONS

In the undefected system the polaron has a pair of intragap levels symmetrically around the Fermi level. We have also seen that the purely dimerized lattice in the presence of a bond defect may (if the defect either strengthens a weak bond or weakens a strong bond) have a pair of intragap states. It is, therefore, not surprising that the polaron and bond impurity may *both* be supported by a single pair of intragap levels which are more localized than either the polaron or defect levels separately. The resulting defect is strongly localized on the bond defect. (If the bond impurity induces ultraband states the impurity and polaron evolve independently asymptotically.)

XI. PHOTOEXCITATION IN THE PRESENCE OF A SINGLE BOND IMPURITY

In the following typical photoexcitation experiments the impurity is of strength $W_0 = -\Delta_0$ and weakens a

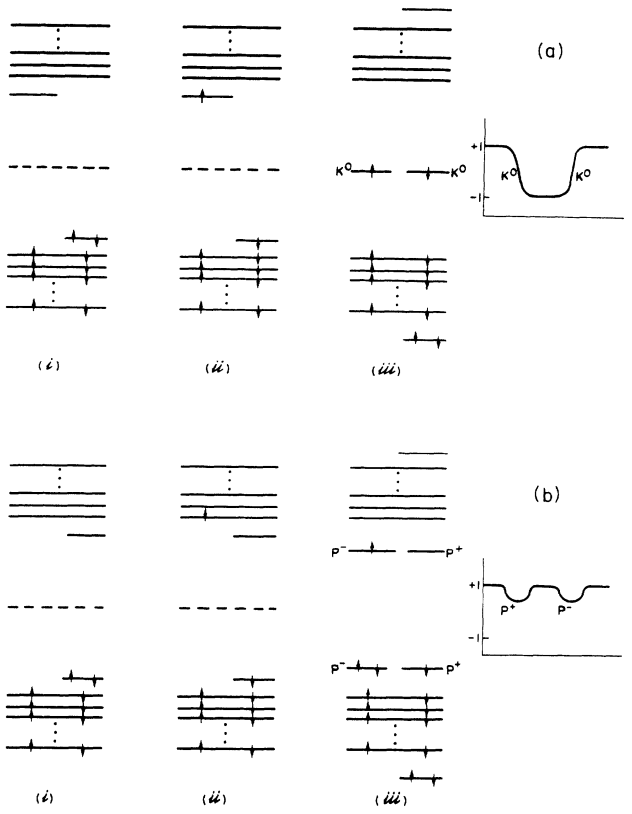

FIG. 14. Schematic of the evolution of the energy levels and order parameter following photoexcitation of a bond-defected system: photoexcitation into (a) the upper impurity level, and (b) the bottom of the conduction band.

strong bond. The initial condition for each is the fully relaxed ground state. Figure 14 shows a schematic of the evolution of the electronic spectrum and lattice during photoexcitation.

A. Adiabatic dynamics

(1) *Neutral impurity: Photoexcitation from lower to upper impurity level.* We have seen that the local impurity-induced lattice distortion is nontopological. Here, where the electronic occupancies are identical with those of photoexcitation in the undefected system, we expect the same qualitative outcome. We find that although the energy added in photoexcitation is $\sim 1.1\Delta_0$ [less than the energy required ($\sim 1.3\Delta_0$) to produce a $K\bar{K}$ pair] the system is again able to produce the $K\bar{K}$ (Fig. 15) pair by removing states from the top of the conduction band and the bottom of the valence band. This appears not to be simply a means of reducing electronic energy in order to produce the $K\bar{K}$ pair, but rather another direct manifestation of the lack of stability of the intragap state. This view is supported by the observation of the production of a breather in addition to a $K\bar{K}$ pair—if the production of ultraband states were merely energy redistribution to allow $K\bar{K}$ production, this would not be expected. Thus the photoexcitation is again very similar to photoexcitation in undefected *trans*-$(CH)_x$: the major difference is a quantitative alteration of the breather produced.

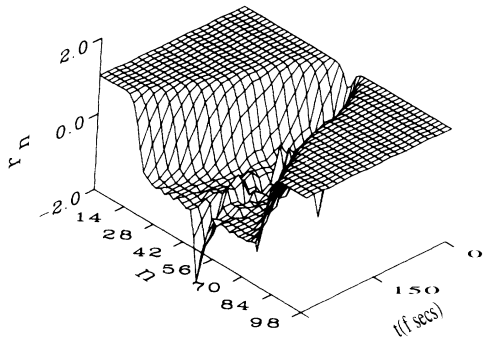

FIG. 15. Photoexcitation of a single electron from the lower to upper impurity level of a strong bond-defected system with defect strength $W_0 = -\Delta_0$.

(2) *Neutral impurity: Photoexcitation from lower impurity level to the bottom of the conduction band.* Again we see that a pair of ultraband states are removed from the band edges. There are two possible evolutions—either to a neutral-positive $K\bar{K}$ pair and an electron polaron, or to both a hole and an electron polaron. In our numerical experiment, the system chooses the branch which produces a pair of polarons symmetrically around the impurity. It is not clear if this branch is decided by kinematic, energetic, or impurity effects. A breather is also produced a long way from the impurity. On the impurity bond itself, there is a complicated lattice distortion with a large amount of localized lattice energy (Fig. 16).

B. Optical absorption

We have calculated the optical absorption of both the ground state and the photoexcited [case (1)] systems above. In Fig. 17 we display the difference, $\Delta\alpha(\omega)$, between the photoinduced absorption of a 98 site ring with and without a single bond impurity. There is a strong

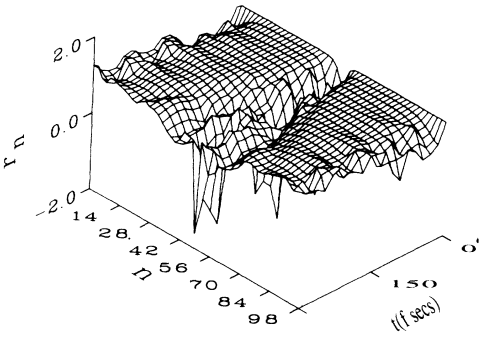

FIG. 16. Photoexcitation of a single electron from the lower impurity level to the bottom of the conduction band for a strong bond-defected system with defect strength $W_0 = -\Delta_0$.

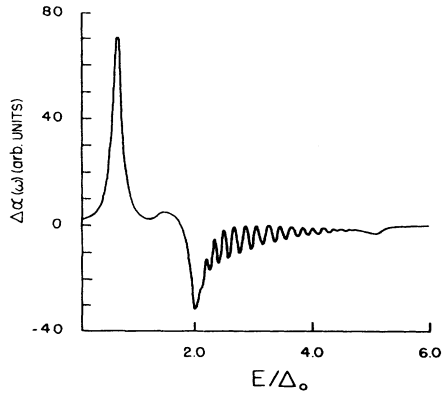

FIG. 17. Difference, $\Delta\alpha(\omega)$, between the absorption of a strong bond-defected system and the purely dimerized lattice.

enhancement at $\sim\Delta_0/4$ arising from transitions between the impurity levels; there is also a smaller, less sharp enhancement at $\sim 3\Delta_0/2$ arising from transitions from the lower impurity level into the conduction band. This is compensated by a shallow broad bleaching above the band edge. Figure 18 shows the difference, $\Delta\alpha(\omega)$, between the absorption after and before photoexcitation. We see a sharp bleaching at $\sim\Delta_0/4$ due to the loss of the transition between the impurity levels. A strong midgap enhancement arises from transitions between the kink midgap levels and the bands; it has a high-energy shoulder arising from transition within a breather. The above-band-edge bleaching compensates for the breather absorption.

XII. SUMMARY AND DISCUSSION

In this paper we have investigated the effects of isolated impurities on the static and dynamic properties of a *trans*-polyacetylene chain described in terms of the SSH model. The impurities have been assumed to couple to the electrons and modeled either as a potential acting on the electron density at a single site ("site impurity") or as a defective hopping matrix element of a particular bond ("bond impurity"). Influences on the lattice dynamics occur only through the electron-phonon coupling.

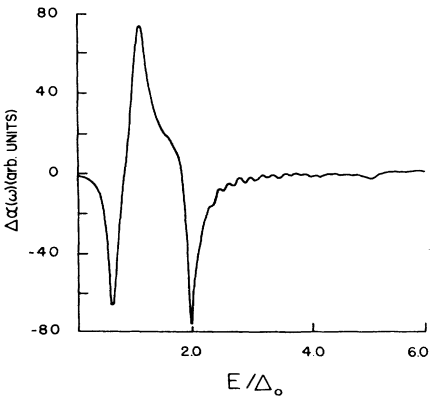

FIG. 18. Change in absorption, $\Delta\alpha(\omega)$, following photoexcitation of a strong bond-defected system.

The equilibrium configurations of the defected system have been analyzed both analytically and numerically. The impurity potentials produce localized electronic states, with levels both in the gap and in the ultraband region, together with lattice distortions in the vicinity of the impurities. Weak potentials ($\lesssim\Delta_0$) induce shallow impurity levels and small distortions. In this case, the system is well described by the analytic expressions for the linear lattice response. The fully self-consistent lattice relaxation, as calculated numerically, simply further enhances localization. Strong impurity potentials ($\gtrsim\Delta_0$) give rise to deep levels initially, but the subsequent lattice relaxation can now qualitatively change the level structure. In fact, we have observed that for sufficiently weakened strong bonds the intragap levels can become less localized. We believe that this strong effect of the lattice distortions corresponds to the situation envisaged in disordered semiconductors some time ago by Anderson:[22] the more localized the electronic states are (due to disorder) the more important is the subsequent self-energy correction due to the electron-phonon interaction. It can even lead to a complete expulsion of levels from the gap. A particularly striking phenomenon is the complete absence of localized gap states for a kink trapped on a sufficiently strong ($|V_0| \gtrsim \Delta_0$) site impurity. These are examples of "hyperdeep" traps[20] where the bonding state ($\sim$ dangling bond) is completely healed by the kink. An important general question which this raises, and which merits further investigation, is the relationship between linear quantum relaxation mechanisms (i.e., phonon emission and/or absorption) and relaxation via adiabatic but nonlinear dynamics. Similar questions arise when considering mechanisms limiting kink velocities in the SSH model:[6] Cerenkov-like linear phonon emission descriptions may be better approached by quantizing nonlinear multiphonon bound states, which constitute the classical relaxation path in these highly nonlinear, low-dimensional systems.

Our studies of collisions between nonlinear excitations (kinks, polarons) and impurities have shown that reflection, transmission, and trapping are all possible, depending on the type of the impurity, its strength, and the velocity of collision. Interestingly, while kinks may be trapped by site defects, polarons may be trapped by bond defects.

Contrary to naive expectations, the presence of strong lattice defects can enhance the production of nonlinear excitations, including some not available to the undefected system. Thus the interaction of a kink with a site impurity can produce a polaron (Sec. V). Again, bond defects act as natural nucleation sites for kink-antikink-breather production in photogeneration experiments. Quite generally photoexcitation into intrinsic (e.g., polaron) or extrinsic (site or bond) gap states, or interband transitions in the presence of such states, provide efficient mechanisms for generating the full spectrum of nonlinear elementary excitations: dynamic kinks (and antikinks), excitons and breathers, as found previously for pure *cis*- and *trans*-polyacetylene models, but also static and dynamic polarons (e.g., Sec. VII and Fig. 10). It is possible that a trapped kink-antikink pair generated simultaneously with a polaron would relax to a metastable state by dissipating

the polaron energy, and would require quantum tunneling for recombination.

It is worthwhile bearing in mind plausible values for impurity strengths in realistic polyacetylene contexts in view of these novel features. V_0 might be as high as ~ 5 eV if due to Coulomb effects in ions, i.e., $\sim(5-10)\Delta_0$, where strong electron-phonon renormalizations are expected. W_0 is small if representative for *cis* segments (~ 0.1 eV $\sim \Delta_0/10$), but large if simulating chain breaks ($\sim t_0$). Several controlled experimental approaches to producing segmented polyacetylenes and other conducting polymers are now developing—including *cis-trans* mixtures, block copolymers, finite polyenes, and selective substitutions. We hope that the present studies will assist in the interpretation of data from these materials: the possibility of trapped kinks on sp^3 defects in partially deuterated *trans*-$(CH)_x$ is already suggested by early data.[23]

The connection between bond or site defects and the widely used concept of "conjugation length" is also worthy of further study. We have noticed that a chain break acts like a barrier from which kinks are reflected over a wide range of energies and polarons may be trapped.

It is appropriate to discuss the possible implications of our results for experiments on pristine or weakly doped polyacetylene. The most immediate impact of impurity gap states is to produce photoabsorption and photoconduction below the direct gap $2\Delta_0$. This has often been attributed to an Urbach tail, i.e., to quantum fluctuations of the phonon field leading to kink-antikink production for photon energies below $2\Delta_0$. This mechanism is outside of the scope of the present adiabatic calculations, but the impurity states will also result in intragap absorption and especially influence long-time photoconduction tails. The photogeneration of polarons close to impurities has interesting consequences for photoconduction since polarons can contribute both to intra- and interchain transport. The efficient photogeneration of kinks and polarons in the presence of defects could bear directly on the controversial question of photoinduced photoabsorption and ESR: (i) polarons are accompanied by spin, and (ii) kink-antikink channels are expected to be dominated by charged (i.e., spinless) species in ideal models. This second statement relies on electron-hole symmetry, which is broken by site defects. The spectroscopic detection of "trapped kinks" which are not accompanied by intragap levels but supported by inert ultraband levels, is an intriguing challenge.[20] (We note that some evidence exists[24] for differences in optical absorption in polyacetylene depending on the dopant species.) Clearly, careful (particularly time-resolved) phototransport, ESR, and absorption experiments will continue to provide key information if samples are well characterized and impurity level can be controlled. For example, differences (e.g., in photogeneration) between compensated and uncompensated samples would be interesting. We note that recent photostudies of polythiophenes[25] have revealed some intragap absorption ascribed to polarons arising from impurity gap states—in addition to intrinsic photoinduced polarons and bipolarons.

We conclude by emphasizing some limitations of our simple modeling of generic bond and site impurity types. The long-range nature of Coulomb fields could well be relevant and modify our results. Also, nonadiabatic effects have been neglected. These could be especially important in the *strong* electron-phonon renormalization regimes we have defined where Franck-Condon effects should be significant (as discussed in a related context by Anderson).[20] Again, it is possible that a trapped-kink-antikink pair (photo)generated simultaneously with a polaron would relax to a metastable state by dissipating the polaron energy, and would require quantum tunneling for recombination. Finally, electron-electron correlation effects are now generally believed to be non-negligible. The interplay of correlations and disorder should be expected to play intricate roles in conjugate polymers—as that they do[26] in other restricted geometry electronic materials such as thin wires or metal-oxide-semiconductor field-effect transistors (MOSFET's); indeed the strong electron-phonon role makes the competitions more interesting, just as in other polaronic contexts.[27]

ACKNOWLEDGMENTS

We are grateful to Peter Vogl for illuminating discussions on the analogies between the site impurity discussed here and isoelectronic impurities in semiconductors. S.R.P. was supported in part by the National Science Foundation through Grant No. DMR-8006311.

APPENDIX A: CONTINUED-FRACTION METHOD

In this appendix we use a continued-fraction scheme[27] to derive the modifications to the band structure due to the presence of a site or bond impurity for a homogeneously dimerized lattice (thus neglecting lattice relaxation effects due to electron-phonon interactions). The local density of states is given by

$$\rho_n(E) = -\frac{1}{\pi}\lim_{\eta\to 0}\mathrm{Im}G_{nn}(E+i\eta)\ , \tag{A1}$$

where $G_{nn}(z)=\langle n\,|\,(z-H)^{-1}\,|\,n\rangle$ is the diagonal matrix element of the resolvent in real-space representation. It can also be viewed as a propagator starting at site n and returning to site n.

For the one-dimensional tight-binding Hamiltonian

$$H=\sum_n \varepsilon_n c_n^\dagger c_n - \sum_n t_{n,n+1}(c_n^\dagger c_{n+1}+c_{n+1}^\dagger c_n)\ , \tag{A2}$$

$G_{nn}(z)$ can be represented as

$$G_{nn}(z)=[z-\varepsilon_n-\Sigma_L(z)-\Sigma_R(z)]^{-1}\ , \tag{A3}$$

where the self-energies Σ_L and Σ_R for propagation to the left and right, respectively, are given by the continued fractions

$$\Sigma_L(z)=\cfrac{t_{n-1,n}^2}{z-\varepsilon_{n-1}-\cfrac{t_{n-1,n-2}^2}{\ddots}}\ , \tag{A4a}$$

$$\Sigma_R(z)=\cfrac{t_{n,n+1}^2}{z-\varepsilon_{n+1}-\cfrac{t_{n+1,n+2}^2}{\ddots}}\ . \tag{A4b}$$

A. Purely dimerized lattice

We consider a dimerized lattice of infinite extent

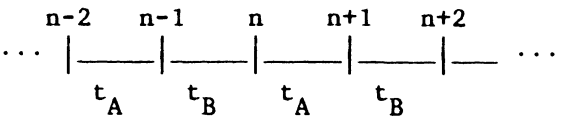

where $t_A = t_0 + \frac{1}{2}(-1)^n \Delta_0$ and $t_B = t_0 - \frac{1}{2}(-1)^n \Delta_0$ with constant on-site energy ($\varepsilon_n = 0$). In this case Eqs. (A3) and (A4) imply that the self-energies for the propagator $G_{nn}(z)$ are related to each other as

$$\Sigma_L = t_B^2/(z - \Sigma_R) , \tag{A5a}$$

$$\Sigma_R = t_A^2/(z - \Sigma_L) , \tag{A5b}$$

giving

$$2z\Sigma_L = z^2 + t_A^2 - t_B^2 \pm [(z^2 + t_A^2 - t_B^2)^2 - 4t_B^2 z^2]^{1/2} . \tag{A6}$$

Equations (A3), (A5), and (A6) yield the following form for the propagator

$$G_{nn}(z) = \pm z/[(z^2 - t_A^2 - t_B^2)^2 - 4t_A^2 t_B^2]^{1/2} . \tag{A7}$$

For $z = E$ the denominator in Eq. (A7) is real and nonzero within the regions

$$E^2 > (t_A^2 + t_B^2) \text{ and } E^2 < |\, t_A^2 - t_B^2 \,| , \tag{A8}$$

but imaginary for

$$|\, t_A^2 - t_B^2 \,| < E^2 < t_A^2 + t_B^2 . \tag{A9}$$

The density of states which vanishes in the former region and is finite in the latter shows the expected band structure: namely bands separated by a gap of width $2\Delta_0$. Equation (A7) leads to the characteristic square-root singularities in the density of states at the band edges.

We still have to determine the appropriate sign of the propagator. Within the region of the bands this is simply accomplished by requiring the density of states to be positive. It follows that the positive sign has to be chosen in Eq. (A7) for $E^2 \geq t_A^2 + t_B^2$, whereas the negative sign is appropriate for $E^2 < t_A^2 + t_B^2$. Another criterion has to be used to determine the appropriate sign for "intragap" and "ultraband" energies. Alternatively, as shown in Appendix B, one can calculate $G_{nn}(z)$ using periodic-boundary conditions and it turns out that the above choice is appropriate for all energies.

B. Site impurity

A site impurity as modeled by Eq. (2) adds energy V_0 to a single site m. Equation (A3) becomes

$$G_{mm}(z) = (z - V_0 - \Sigma_L - \Sigma_R)^{-1} , \tag{A10}$$

with Σ_L and Σ_R as given in Eqs. (A5) and (A6). We find the same positions for the band edges as in the pure system. However, there is a possibility of further contributions to the density of states at the poles of $G_{mm}(z)$, i.e., for energies satisfying the equation

$$E - V_0 - \Sigma_L(E) - \Sigma_R(E) = 0 . \tag{A11}$$

Taking into account the appropriate signs in (A7), as derived previously, we obtain the solutions given in Eq. (4). It is easy to convince oneself that these solutions correspond to a positive density of states.

C. Bond impurity

A bond impurity as modeled by Eq. (3) modifies the transfer matrix $t_{m,m+1} = t_A$ to $t_E = t_A + W_0$. The propagator (A3) becomes

$$G_{mm}(z) = (z - \Sigma_L - \Sigma_R')^{-1} , \tag{A12}$$

where

$$\Sigma_R' = (t_E/t_A)^2 \Sigma_R , \tag{A13}$$

with Σ_L and Σ_R still given by Eqs. (A5) and (A6). Again the positions of the band edges are not changed. Additional states are found as solutions of the equation

$$E - \Sigma_L(E) - (t_E/t_A)^2 \Sigma_R(E) = 0 . \tag{A14}$$

We find pairs of solutions $\pm |\, E \,|$ with

$$|\, E \,| = \frac{1}{2\,|\, t_E \,|} \left| \, t_E^2 + t_A^2 \pm [(t_E^2 - t_A^2)^2 + 4t_E^2 t_B^2]^{1/2} \right| . \tag{A15}$$

The plus and minus signs in (A15) correspond to pairs of ultraband and of intragap states, respectively. The appropriate signs in Eq. (A7) (plus for the ultraband, minus for the intragap region) specify the parameters for which the solutions (A15) occur. Ultraband states are found if $|\, t_E \,| > t_A$ whereas intragap states develop either if $t_A > |\, t_E \,|$ and $t_A > t_B$ or if $t_A < |\, t_E \,|$ and $t_A < t_B$.

APPENDIX B: GREEN'S FUNCTIONS FOR SITE AND BOND IMPURITIES AND LINEAR LATTICE RELAXATION

The electronic Green's functions

$$G_{mn}(iE) = \langle m \,|\, (iE - H_{\rm el})^{-1} \,|\, n \rangle , \tag{B1}$$

where $H_{\rm el}$ is the electronic part of the Hamiltonian, determine the impurity-induced lattice relaxation, as shown in Sec. III. In the following we will evaluate these functions for a purely dimerized lattice. This yields the linear response of the lattice to the impurity-induced changes in the electronic structure.

A. Pure case ($H_1 = H_2 = 0$)

For later use we determine first the Green's functions $G_{mn}^0(iE)$ for the pure system which is described by the Hamiltonian

$$H_0 = -\sum_n [t_0 + \tfrac{1}{2}(-1)^n \Delta_0](c_n^\dagger c_{n+1} + \text{H.c.}) , \tag{B2}$$

where $n = 1, \ldots, n$ and $c_{N+1} \equiv c_1$. The canonical transformation

$$c_n = (-i)^n N^{-1/2} \sum_k \exp\{i[kn - (-1)^n \theta_k]\} \times [(-1)^n a_k + b_k] , \tag{B3}$$

where $-\pi/2<k\leq\pi/2$ and a_k, b_k are fermion operators, diagonalizes H_0 if θ_k satisfies the relation

$$2t_0\tan(2\theta_k)=\Delta_0\cot k \ . \tag{B4}$$

H_0 assumes the form

$$H_0=\sum_k \mathrm{sgn}(k)E_k(a_k^\dagger a_k - b_k^\dagger b_k) \ , \tag{B5}$$

where

$$E_k=(4t_0^2\sin^2 k+\Delta_0^2\cos^2 k)^{1/2} \ . \tag{B6}$$

It is straightforward to calculate the Green's functions $G^0_{nm}(iE)$ using Eqs. (B3)–(B5). We find

$$G^0_{mn}(iE)=-iE[(E^2+4t_0^2)(E^2+\Delta_0^2)]^{-1/2} \times(-1)^{(m-n)/2}q^{|m-n|/2} \ , \tag{B7a}$$

if n-m is even and

$$G^0_{mn}(iE)=(4t_0^2-\Delta_0^2)^{-1/2}[(-1)^{(m+n-1)/2}\Delta_0(E^2+\Delta_0^2)^{-1/2}+(-1)^{(|m-n-1|)/2}2t_0(E^2+4t_0^2)^{-1/2}]q^{|m-n|/2} \ , \tag{B7b}$$

if n-m is odd, where

$$q=[(E^2+4t_0^2)^{1/2}-(E^2+\Delta_0^2)^{1/2}]/[(E^2+4t_0^2)^{1/2}+(E^2+\Delta_0^2)^{1/2}] \ . \tag{B8}$$

These functions are symmetric

$$G^0_{mn}(iE)=G^0_{nm}(iE) \ . \tag{B9}$$

B. Site impurity

The Green's function for the site impurity has already been discussed in Ref. 11. For $H_{\mathrm{el}}=H_0+H'$ the operator $(z-H_{\mathrm{el}})^{-1}$ can be generally written as

$$(z-H_{\mathrm{el}})^{-1}=(z-H_0)^{-1}\sum_{j=0}^{\infty}[H'(z-H_0)^{-1}]^j \ . \tag{B10}$$

For the particular case $H'=H_1$ [Eq. (2)] the summation is easily carried out giving

$$G_{ln}(z)=G^0_{ln}(z)+G^0_{lm}(z)\frac{V_0}{1-V_0G^0_{mm}(z)}G^0_{mn}(z) \ , \tag{B11}$$

where G^0_{mn} is given by Eqs. (B7).

C. Bond impurity

We start again from Eq. (B10) with $H'=H_2$, represented in first-quantized form

$$H_2=-W_0(|m\rangle\langle m+1|+|m+1\rangle\langle m|) \ . \tag{B12}$$

Similarly, we can write

$$[H_2(z-H_0)^{-1}]^jH_2=(-W_0)^{j+1}[p_j(|m\rangle\langle m|+|m+1\rangle\langle m+1|+q_j(|m\rangle\langle m+1|+|m+1\rangle\langle m|)] \ , \tag{B13}$$

where the coefficients p_j and q_j are determined by induction. We find

$$p_j=\tfrac{1}{2}[(g_1+g_0)^j-(g_1-g_0)^j] \ , \tag{B14a}$$

$$q_j=\tfrac{1}{2}[(g_1+g_0)^j+(g_1-g_0)^j] \ , \tag{B14b}$$

where $g_0=G^{(0)}_{mm}=G^{(0)}_{m+1,m+1}$ and $g_1=G^{(0)}_{m,m+1}=G^{(0)}_{m+1,m}$. Combining Eqs. (B1), (B10), (B13), and (B14), we finally obtain

$$G_{ln}=G^0_{ln}-\frac{W_0}{(1+W_0g_1)^2-(W_0g_0)^2}[(1+W_0g_1)(G^0_{lm}G^0_{m+1,n}+G^0_{l,m+1}G^0_{mn})-W_0g_0(G^0_{lm}G^0_{mn}+G^0_{l,m+1}G^0_{m+1,n})] \ . \tag{B15}$$

D. Linear response of the lattice

The knowledge of the electronic Green's functions both for the pure and impure systems allows us to calculate the impurity-induced lattice distortion $\Delta_n-\Delta_0$ through Eq. (10). Introducing the integration variable

$$x=[(E^2+4t_0^2)/(E^2+\Delta_0^2)]^{1/2} \tag{B16}$$

and using Eqs. (B7) and (B11), we find for a site impurity at m

$$(\Delta_n-\Delta_0)/\Delta_0=-2\lambda\xi(V_0/\Delta_0)^2 \times\int_1^{\xi}dx\,f(x)(\pm\sigma_m\xi+x) \times[(x-1)/(x+1)]^{|n-m+(1/2)|} \ , \tag{B17}$$

where

$$f(x)=(\xi^2-x^2)^{1/2}/[x^2(\xi^2-1)^2 +(V_0/\Delta_0)^2(\xi^2-x^2)(x^2-1)] \ , \tag{B18a}$$

$$\sigma_m=(-1)^m\ , \tag{B18b}$$

and the upper and lower signs correspond to $n \geq m$ and $n < m$, respectively. Equation (B17) implies that both bonds neighboring the impurity site are weakened. This leads to an overall expansion of the lattice. To calculate the displacements u_n we use the relation

$$\Delta_n=2\alpha(-1)^n(u_n-u_{n+1}) \tag{B19}$$

and obtain the two expressions

$$u_n=u_+ +(-1)^n u_0\left[1+2\sum_{k=0}^{\infty}(-1)^k(\Delta_{n+k}-\Delta_0)/\Delta_0\right]\ , \tag{B20a}$$

$$u_n=u_- +(-1)^n u_0\left[1+2\sum_{k=0}^{\infty}(-1)^k(\Delta_{n-k-1}-\Delta_0)/\Delta_0\right]\ , \tag{B20b}$$

where u_+ and u_- are the overall shifts for $n\to+\infty$ and $n\to-\infty$, respectively. Using (B20a) for $n \geq m$ and (B20b) for $n \leq m$ and performing the (B20a) and (B20b) summations, we find

$$u_n=u_\pm +(-1)^n u_0\left[1-2\lambda\xi(V_0/\Delta_0)^2\int_1^\xi dx(x^2-1)^{1/2}f(x)[1\pm\sigma_m\xi/x][(x-1)/(x+1)]^{|n-m|}\right]\ , \tag{B21}$$

where the upper and lower signs correspond to $n \geq m$ and $n \leq m$, respectively. Identifying the two expressions for $n=m$ leads to the following result for the overall expansion

$$u_+ -u_- =4\lambda\xi^2 u_0(V_0/\Delta_0)^2\int_1^\xi dx(x^2-1)^{1/2}f(x)/x\ . \tag{B22}$$

Proceeding in the same way for a bond impurity between sites m and $m+1$ and using Eqs. (10), (B7), (B15), and (B16), we find for $n\neq m$

$$(\Delta_n-\Delta_0)/\Delta_0=4\lambda\sigma_m w\xi(\xi-\sigma_m)(\xi+\sigma_m+w)\int_1^\xi dx\, g_1(x)[(x-1)/(x+1)]^{|n-m|}/h(x)\ , \tag{B23}$$

where

$$w=W_0/\Delta_0\ , \tag{B24a}$$

$$g_1(x)=x[(\xi^2-x^2)/(x^2-1)]^{1/2}\ , \tag{B24b}$$

$$h(x)=[x(\xi^2-1)+w(x-1)(\xi+\sigma_m x)]^2+w^2(\xi^2-x^2)(x^2-1)\ . \tag{B24c}$$

The local relaxation at the defect bond is obtained as

$$(\Delta_m-\Delta_0)/\Delta_0=4\lambda\sigma_m w\xi(\xi-\sigma_m)\int_1^\xi dx\, g_2(x)/h(x)\ , \tag{B25}$$

where

$$g_2(x)=x[(\xi+\sigma_m x)/(\xi-\sigma_m x)]^{1/2}(x-1)^{-1/2}(x+1)^{-3/2}[(\xi+\sigma_m)(\xi-\sigma_m x^2)-w(\xi+\sigma_m x)(x-1)]\ . \tag{B26}$$

The integral (B25) is dominated by the contributions around $x=1$. Therefore, writing the effective transfer integral $t_{m,m+1}$ as

$$t_{m,m+1}=t_0+\tfrac{1}{2}\sigma_m\Delta_0[1+2\sigma_m w+(\Delta_m-\Delta_0)/\Delta_0]\ , \tag{B27}$$

we realize that the lattice relaxation tends to increase the effect of the impurity potential. It follows that the localization of intragap and ultraband states is further enhanced. The displacements u_n are calculated in the same way as for the site impurity. Using Eq. (B20a) for $n>m$ and Eq. (B20b) for $n \leq m$, we find

$$u_n=u_\pm +(-1)^n u_0[1+4\lambda\sigma_m w\xi(\xi-\sigma_m)(\xi+\sigma_m+w)\int_1^\xi dx(x\pm1)g_1(x)[(x-1)/(x+1)]^{|n-m|}/(xh(x))\ , \tag{B28}$$

where the upper and lower signs correspond to $n>m$ and $n \leq m$, respectively. The overall shift $u_+ -u_-$ is calculated by requiring Eq. (B28) to be consistent with Eq. (B25). This gives

$$u_+ -u_- =8\lambda u_0 w\xi(\xi-\sigma_m)\int_1^\xi dx[(\xi+\sigma_m+w)(x-1)g_1(x)-xg_2(x)]/(xh(x))\ . \tag{B29}$$

Choosing a symmetric overall expansion (or contraction), $u_{\pm}=\pm u_a$, Eqs. (B21) and (B28) can be represented in the form of Eq. (11) with $2u_a$ given by Eqs. (B22) and (B29) for the site and bond impurities, respectively.

APPENDIX C: MOLECULAR DYNAMICS TECHNIQUE

In this appendix we describe our mean-field adiabatic molecular dynamics technique in detail. The adiabatic (Born-Oppenheimer) approximation assumes that the motion of the ions is described by well-defined trajectories following Newton's law. This approximation is valid when the Fermi velocity is much larger than the sound velocity. For the parameter values used here we have $v_F/v_s=20$. The equation of motion for the ions is then:

$$m\ddot{u}_n=\mathcal{F}_n \ , \tag{C1}$$

where $\mathcal{F}_n$ is the time-dependent effective force acting on the nth ion, arising from occupied electronic states and harmonic lattice interaction. The force is thus generated by the potential

$$V(\{u_n\})=E_0(\{u_n\})+\frac{K}{2}\sum_n(u_{n+1}-u_n)^2 \ . \tag{C2}$$

The term $E_0(\{u_n\})$, the electronic energy for a given ion configuration $\{u_n\}$, can be calculated as the sum of the occupied one-electron energies:

$$E_0(\{u_n\})=\sum_{\nu,\sigma} m_{\nu,\sigma}\varepsilon_{\nu,\sigma} \ . \tag{C3}$$

Here $m_{\nu,\sigma}$ is the occupation number of state ν with spin σ and the sum is over all occupied states. The problem is now to find the one-electron energies, given an ion configuration $\{u_n\}$, a total chain length N, and the number of electrons in the system. Since polyacetylene has one π electron per CH group, there is exactly one electronic state per site. The π orbitals can thus conveniently be chosen as a truncated basis set. The one-electron energies can now be found by direct diagonalization of the $N\times N$ transfer matrix $T(\{u_n\})$, with matrix elements:

$$T_{i,j}=[t_0+\alpha(u_i-u_j)][\delta_{i,j-1}+\delta_{i,j+1}] \ , \tag{C4}$$

where $(i,j)=1,2,\ldots,N$. Once the potential $V(\{u_n\})$ is known the force F_n in Eq. (C1) is found as the functional derivative

$$\mathcal{F}_n=-\frac{\delta V(\{u_n\})}{\delta u_n} \ . \tag{C5}$$

$\mathcal{F}_n$ is now known and Eq. (C1) is integrated by the standard Verlet algorithm[26] (leap-frog, second-order central difference scheme). If we discretize time in steps Δt, we have $u_n(t)=u_n(k\Delta t)\equiv u_n^k$ and for Eq. (1),

$$u_n^{k+1}-2u_n^k+u_n^{k-1}=\frac{(\Delta t)^2\mathcal{F}_n}{m} \ . \tag{C6}$$

The Verlet scheme is very efficient and quite accurate. The energy is typically conserved to within 0.5% with no significant systematic drift. A higher-order predictor-corrector scheme would no doubt be more accurate but would also require substantially more computer time and storage. The Beeman algorithm,[28] which has also been used to some extent in conventional molecular-dynamics (MD) calculations, has a slightly different definition of the velocity, but can be shown[29] to produce the same trajectories as Eq. (C6); it is however more costly to compute.

In some cases it is useful to "relax" the system by removing kinetic energy (see main text). This is done by resetting the velocity to zero at each time step (i.e., $u_n^k=u_n^{k-1}$). In this case Eq. (C6) is changed to

$$u_n^{k+1}-u_n^k-\frac{(\Delta t)^2\mathcal{F}_n}{m} \ . \tag{C7}$$

The numerical algorithm now consists of the following steps: (1) Prescribe a given ion configuration $\{u_n\}$ and the number of electrons on a chain of length N. The $t=0$ and $t=1$ lattice configurations must be prescribed to initialize the code. (2) Diagonalize $T(\{u_n\})$. (3) Compute $V(\{u_n\})$. (4) For a given n: change $u_n\rightarrow u_n+\delta$. (5) Diagonalize $T(\{u_n+\delta\})$. (6) Compute $V(\{u_n+\delta\})$. (7) Compute

$$\mathcal{F}_n=-\frac{\delta V(\{u_n\})}{\delta u_n}\sim\frac{V(\{u_n+\delta\})-V(\{u_n\})}{\delta} \ .$$

(8) Change n to $n+1$ and repeat from step (4) for all n in $[1,N]$. (9) Time integrate Eq. (1) one time step Δt to find the new $\{u_n\}$, i.e., $\{u_n(t+\Delta t)\}$. Repeat from step (2).

In addition to already mentioned parameter values (see Sec. I), we have used $\Delta t=10^{-15}$ sec and $\delta=0.001$ throughout this study.

---

*Also at Physics Department, University of Florida, Gainesville, FL 32611. Present address: Materials Science Division, Argonne National Laboratory, Argonne, IL 60439.

†Permanent address: Institut für Theoretische Physik, Eidgenössische Technische Hochschule Zürich—Hönggerberg, CH-8093 Zürich, Switzerland.

[1]S. Etemad, A. J. Heeger, and A. G. MacDiarmid, Ann. Rev. Phys. Chem. **33**, 443 (1982).

[2]D. Baeriswyl, G. Harbeke, H. Kiess, and W. Meyer, in *Electronic Properties of Polymers*, edited by J. Mort and G. Pfister (Wiley, New York, 1982), p. 267.

[3]W. P. Su, J. R. Schrieffer, and A. J. Heeger, Phys. Rev. B **22**, 2099 (1980), **28**, 1138(E) (1983).

[4]H. Takayma, Y. R. Lin-Liu, and K. Maki, Phys. Rev. B **21**, 2388 (1980); B. Horovitz, *ibid.* **22**, 1101 (1980); S. A. Brazovskii and N. N. Kirova, Sov. Sci. Rev. A Phys. **5**, 99 (1984).

[5]W. P. Su and J. R. Schrieffer, Proc. Natl. Acad. Sci. **77**, 5626 (1980).

[6]A. R. Bishop, D. K. Campbell, P. S. Lomdahl, B. Horovitz, and S. R. Phillpot, Phys. Rev. Lett. **52**, 671 (1984), Synth. Metals **9**, 223 (1984).

[7]F. Guinea, Phys. Rev. B **30**, 1884 (1984).

[8]S. R. Phillpot, A. R. Bishop, B. Horovitz, and P. S. Lomdahl (unpublished); S. R. Phillpot, Doctoral dissertation, University of Florida, 1985. Here we restrict ourselves to time-averaged adiabatic optical absorption. Limitations of this scheme for dynamic processes and nonadiabatic corrections are discussed in the above report.

[9]J. Orenstein, Z. Vardeny, and G. L. Baker, J. Phys. (Paris) Colloq. **44**, C3-407 (1983); Z. Vardeny, J. Orenstein, and G. L. Baker, *ibid.* **44**, C3-325 (1983); J. Orenstein, in *Handbook of Conducting Polymers,* edited by T. A. Skotheim (Marcel Dekker, New York, 1986).

[10]M. Tokumoto, H. Oyanagi, T. Ishiguro, H. Shirakawa, H. Nemoto, T. Matsushita, M. Ito, H. Kuroda, and K. Kohra, Solid State Commun. **48**, 861 (1983).

[11]D. Baeriswyl, J. Phys. (Paris) Colloq. **44**, C3-381 (1983); and unpublished.

[12]E. J. Mele and M. J. Rice, Phys. Rev. B **23**, 5397 (1981).

[13]C. T. White, M. L. Elert, and J. W. Mintmire, J. Phys. (Paris) Colloq. **44**, C3-481 (1983).

[14]G. W Bryant and A. J. Glick, Phys. Rev. B **26**, 5855 (1982).

[15]A. R. Bishop and D. K. Campbell, in *Nonlinear Problems: Present and Future,* edited by A. R. Bishop, D. K. Campbell, and B. Nicolaenko (North-Holland, Amsterdam, 1982), p. 195.

[16]J. Sethna and S. Kivelson, Phys. Rev. B **26**, 3513 (1982); **27**, 7798(E) (1983); Z. Su and Lu Yu, *ibid.* **27**, 5199 (1983); **29**, 2309(E) (1984).

[17]A. R. Bishop, D. K. Campbell, P. S. Lomdahl, S. R. Phillpot, D. Baeriswyl, and B. Horovitz, Mol. Cryst. Liq. Cryst. **118**, 65 (1985); S. R. Phillpot, D. Baeriswyl, A. R. Bishop, and P. S. Lomdahl, Synth. Metals **13**, 129 (1986); in this paper the impurity levels for the site impurity are in error (factors of 2).

[18]For example, G. A. Baratoff, E. O. Kane, and M. Schlüter, Phys. Rev. B **21**, 5662 (1980).

[19]D. K. Campbell, J. F. Schonfeld, and C. A. Wingate, Physica **9D**, 1 (1983).

[20]P. Vogl, in Festkörperprobleme **21**, 191 (1981).

[21]K. Fesser, A. R. Bishop and D. K. Campbell, Phys. Rev. B **27**, 4804 (1983).

[22]P. W. Anderson, Nature **235**, 163 (1972). Note that this paper considers the influence of a *site* impurity in a molecular crystal model (i.e., *intra*-molecular phonon coupling). We have found here similar effects for a *bond* impurity in the SSH model (i.e., *inter*molecular phonon coupling).

[23]For example, F. Zuo, A. J. Epstein, X.-Q. Yang, D. B. Tanner, G. Arbuckle, and A. G. MacDiarmid (unpublished).

[24]H. Kiess, G. Harbeke, B. J. Curtis, and R. Keller, J. Phys. (Paris) Colloq. **44**, C3-285 (1983).

[25]Z. Vardeny, E. Ehrenfreund, O. Brafman, M. Nowak, H. Schaffer, A. J. Heeger, and F. Wudl, Phys. Rev. Lett. **56**, 671 (1986).

[26]P. A. Lee and R. V. Ramakrishnan, Rev. Mod. Phys. **57**, 287 (1985).

[27]See, D. Emin, Physics Today **35**(6), 34 (1982).

[28]E. N. Economou and M. H. Cohen, Phys. Rev. B **4**, 396 (1974); S. Y. Wu, C. C. Tung, and M. Schwartz, J. Math. Phys. **15**, 938 (1974); A. R. Bishop, Solid State Commun. **33**, 955 (1980).

[29]R. W. Hockney and J. W. Eastwood, *Computer Simulation Using Particles* (McGraw-Hill, New York, 1981).